DOI 10.1007/s11029-019-09825-w
Mechanics of Composite Materials, Vol. 55, No. 4, September, 2019 (Russian Original Vol. 55, No. 4, July-August, 2019)

SYMPLECTIC METHOD-BASED ANALYSIS OF AXISYMMETRIC DYNAMIC THERMAL BUCKLING OF FUNCTIONALLY GRADED CIRCULAR PLATES

J. H. Zhang,[1*] X. Liu,[1] and X. Zhao[2]

Keywords: *functionally graded materials, dynamic stability, thermal buckling, symplectic method*

The dynamic thermal buckling of circular thin plates made of a functionally graded material is investigated by the symplectic method. Based on the Hamilton principle, canonical equations are established in the symplectic space, and the problems of axisymmetric dynamic thermal buckling of the plates are simplified. The buckling loads and modes of the plates are translated into generalized eigenvalues and eigensolutions, which can be obtained from bifurcation conditions. The effects of gradient properties, parameters of geometric shape, and dynamic thermal loads on the critical temperature increments are considered.

1. Introduction

Functionally graded materials (FGMs) are new composites which are often made of metals and ceramics. Their properties vary smoothly and continuously according to the gradually changing volume fractions of constituent materials. The structures made of FGMs can successfully minimize the thermal stresses, therefore, they can be used in extreme thermal environments [1, 2].

The stability of FGM structures have been studied extensively, particularly the thermal buckling behavior of FGM beams, plates, and shells. However, most of previous studies only dealt with static problems [3-13]. For example, a shooting method-based analysis of buckling and postbuckling of FGM Timoshenko beams and imperfect FGM plates was performed by Li et al. [4, 5]. The thermal postbuckling of uniform slender FGM beams was investigated by Anandrao et al.

[1]School of Science, Lanzhou University of Technology, Lanzhou 730050, P.R.China
[2]Taiyuan Boiler Group Co.,Ltd, Taiyuan 030000, P.R.China
[*]Corresponding author; e-mail: zhangjinghua@mail.xjtu.edu.cn

Russian translation published in Mekhanika Kompozitnykh Materialov, Vol. 55, No. 4, pp. 663-676, July-August, 2019. Original article submitted August 16, 2018; revision submitted January 22, 2019.

[6] using the Rayleigh–Ritz and finite-element methods. The nonlinear thermal buckling and postbuckling of FGM tubes and beams were examined by She et al. [7, 8], with transverse shear and temperature effects considered. In addition, studies on the thermal postbuckling of circular FGM plates were carried out by Ma and Wang [9, 10]. Considering temperature and size effects, the thermal-mechanical-electrical buckling characteristics of FGM microbeams were investigated by Jia et al. [11]. Based on the symplectic method, Sun et al. [12, 13] studied the static buckling behavior of compressed FGM cylindrical shells subjected to thermal loads.

However, studies into the dynamic thermal buckling of the FGM structures are fewer in number than those dealing with static buckling. Mirzavand et al. [14] investigated the dynamic postbuckling characteristics of piezoelectric FGM cylindrical shells under thermal loads on the basis of Budiansky stability criterion. Mirzavand et al. [15] studied the dynamic thermal postbuckling and buckling of FGM cylindrical shells on the basis of a third-order shell theory. Shariyat [16] analyzed the nonlinear dynamic buckling characteristics of suddenly heated FGM cylindrical shells. The dynamic buckling behavior of FGM plates under thermal, electric, and mechanical loads was also examined by Shariyat [17]. Bich et al. [18] examined the dynamic buckling of stiffened FGM cylindrical shells under different types of compressive loads. Using the Galerkin method and considering the damping effect, the nonlinear dynamic buckling of FGM stiff and soft cylindrical shells was studied by Gao et al. [19].

To the best of our knowledge, only few research results have been reported on the dynamic thermal stability of circular FGM plates. Therefore, in this study, the dynamic thermal buckling behavior of thin plates is examined. Based on the symplectic method in the Hamilton system [20, 21], the equations of structural stability problems are solved by means of variable separation and expansion in symplectic eigenfunctions.

2. Mathematical Formulation of Problem

2.1. Fundamental problem

Circular FGM plates of thickness h and radius R are considered. They are in the initial steady-state heat balance and are subjected to a uniform dynamic thermal load on their bottom surfaces, while their upper surfaces exchange heat with surroundings. The initial displacements and their rates are zero at all points. The dynamic thermal load is assumed in the form $T\left(-h/2,t\right)=\Delta T\cdot f\left(t\right)$, where ΔT is its amplitude and the function $f\left(t\right)$ describes temperature variations. The dynamic thermal buckling of the plates will be investigated in cylindrical coordinates $\left(r,\theta,z\right)$, where r and θ are the radial and circumferential directions. The distance from the plate middle plane is measured along the z coordinate.

The plates are made from a ceramic and metal, whose volume fractions vary in the thickness direction according to specified functions. The upper surfaces are metallic and the bottom ones are ceramic. Based on the rule of mixtures, the material properties $P(z)$ of the structures (including Young's modulus E, density ρ, the specific heat capacity C, the coefficient of thermal expansion α, and the coefficient of thermal conductivity K) vary continuously from those of ceramic to those of metal across the thickness direction according to the same relations as in [22]. The volume fractions vary as power functions, which are also given in [22], where the power-law index k represents the gradient properties of FGM. Usually, Poisson's ratio ν varies little, and it was considered constant, $\nu(z)=\nu$ [22]. To facilitate the analysis of heat conduction in the plates, all material properties were expanded into the Taylor series with respect to z about midplanes of the plates:

$$\left[E,\alpha,K,\left(\rho C\right)\right]=\sum_{n=0}^{\infty}\left[\tilde{E}_n,\tilde{\alpha}_n,\tilde{K}_n,\tilde{\zeta}_n\right]z^n \tag{1}$$

where the coefficients in the right side of Eqs. (1) are specified as

$$\left[\tilde{E}_n, \tilde{\alpha}_n, \tilde{K}_n, \tilde{\zeta}_n\right] = \frac{1}{n!}\left[E^{(n)}(0), \alpha^{(n)}(0), K^{(n)}(0), [\rho C]^{(n)}(0)\right].$$

2.2. Fundamental equations

Strains of the FGM circular plates can be regarded as axisymmetric owing to the uniform dynamic thermal loads imposed on their bottom surfaces. According to the classical plate theory, the axisymmetric geometric equations of the FGM circular plates in a cylindrical coordinate system are given by [10]

$$\varepsilon_r = \varepsilon_r^0 + z\kappa_r, \quad \varepsilon_\theta = \varepsilon_\theta^0 + z\kappa_\theta, \tag{2a}$$

$$\varepsilon_r^0 = \frac{\partial u}{\partial r}, \quad \varepsilon_\theta^0 = \frac{u}{r}, \quad \kappa_r = -\frac{\partial^2 w}{\partial r^2}, \quad \kappa_\theta = -\frac{1}{r}\frac{\partial w}{\partial r}, \tag{2b}$$

where $u(r,t)$ and $w(r,t)$ are displacements in the r and z directions; t is time; ε_r and ε_θ are the normal strains at an arbitrary point in the r and θ directions, respectively; ε_r^0 and ε_θ^0 are the normal strains on plate midplanes; κ_r and κ_θ are curvatures. The boundary of the plates is fixed, and the boundary conditions are $w = 0$ and $\frac{\partial w}{\partial r} = 0$ at $r = R$.

Assuming that the functionally graded materials are linearly thermoelastic, the constitutive equations are expressed as [5]

$$\sigma_r = \frac{E(z)(\varepsilon_r + \nu\varepsilon_\theta)}{1-\nu^2} - \frac{E(z)\alpha(z)T(z,t)}{1-\nu}, \tag{3a}$$

$$\sigma_\theta = \frac{E(z)(\varepsilon_\theta + \nu\varepsilon_r)}{1-\nu^2} - \frac{E(z)\alpha(z)T(z,t)}{1-\nu}, \tag{3b}$$

where σ_r and σ_θ are the normal stresses in the r and θ directions, and $T(z,t)$ is the temperature increment relative to the reference temperature $T_0 = 300$ K. Integrating σ_r and σ_θ across the plate thickness, the membrane forces and bending moments are obtained as

$$\{N_x, N_\theta, M_x, M_\theta\}^{\mathrm{T}} = \int_{-h/2}^{h/2} \{\sigma_x, \sigma_\theta, z\sigma_x, z\sigma_\theta\}^{\mathrm{T}} \,\mathrm{d}z. \tag{4a}$$

Inserting Eqs. (2) and Eqs. (3) into Eqs (4a), the membrane forces and moments are expressed as

$$\begin{Bmatrix} N_x \\ N_\theta \end{Bmatrix} = A\begin{bmatrix} 1 & \nu \\ \nu & 1 \end{bmatrix}\begin{Bmatrix} \varepsilon_x^0 \\ \varepsilon_\theta^0 \end{Bmatrix} + D\begin{bmatrix} 1 & \nu \\ \nu & 1 \end{bmatrix}\begin{Bmatrix} \kappa_x \\ \kappa_\theta \end{Bmatrix} - N^T, \tag{4b}$$

$$\begin{Bmatrix} M_x \\ M_\theta \end{Bmatrix} = D\begin{bmatrix} 1 & \nu \\ \nu & 1 \end{bmatrix}\begin{Bmatrix} \varepsilon_x^0 \\ \varepsilon_\theta^0 \end{Bmatrix} + B\begin{bmatrix} 1 & \nu \\ \nu & 1 \end{bmatrix}\begin{Bmatrix} \kappa_x \\ \kappa_\theta \end{Bmatrix} - M^T, \tag{4c}$$

where N^T and M^T are the thermal membrane force and thermal moment. A, D, and B are stiffness coefficients, which are defined as

$$\{A, D, B\}^{\mathrm{T}} = \int_{-h/2}^{h/2} \frac{E}{1-\nu^2}\{1, z, z^2\}^{\mathrm{T}} \,\mathrm{d}z. \tag{5}$$

2.3. Canonical equations

For the FGM plates, only the energy U of bending strains is considered owing to its dominance. This energy is expressed as

$$U=\frac{1}{2}\int_V\left(\sigma_r\varepsilon_r+\sigma_\theta\varepsilon_\theta\right)\mathrm{d}V$$

$$=\frac{1}{2}\int_0^{2\pi}\int_0^R\left[B\left(\kappa_r+\kappa_\theta\right)^2-2\left(1-\nu\right)B\kappa_r\kappa_\theta-M^T\kappa_r-M^T\kappa_\theta\right]r\mathrm{d}r\mathrm{d}\theta\ .$$

The relevant density of strain energy is

$$\bar{U}=\frac{1}{2}\left[B\left(\kappa_r+\kappa_\theta\right)^2-2\left(1-\nu\right)B\kappa_r\kappa_\theta-M^T\kappa_r-M^T\kappa_\theta\right].$$

Inserting Eqs. (2) into the previous expression yields

$$\bar{U}=\frac{1}{2}B\left(\frac{\partial^2w}{\partial r^2}+\frac{1}{r}\frac{\partial w}{\partial r}\right)^2-\left(1-\nu\right)B\frac{1}{r}\frac{\partial w}{\partial r}\frac{\partial^2w}{\partial r^2}+\frac{1}{2}M^T\left(\frac{\partial^2w}{\partial r^2}+\frac{1}{r}\frac{\partial w}{\partial r}\right) \tag{6}$$

The Lagrange function of the plates is

$$l=\frac{1}{2}I_0\left(\frac{\partial w}{\partial t}\right)^2-\bar{U}+\frac{1}{2}N^T\left(\frac{\partial w}{\partial r}\right)^2=\frac{1}{2}I_0\left(\frac{\partial w}{\partial t}\right)^2-\frac{1}{2}B\left(\frac{\partial^2w}{\partial r^2}+\frac{1}{r}\frac{\partial w}{\partial r}\right)^2$$

$$+\left(1-\nu\right)B\frac{1}{r}\frac{\partial w}{\partial r}\frac{\partial^2w}{\partial r^2}-\frac{1}{2}M^T\left(\frac{\partial^2w}{\partial r^2}+\frac{1}{r}\frac{\partial w}{\partial r}\right)+\frac{1}{2}N^T\left(\frac{\partial w}{\partial r}\right)^2, \tag{7}$$

where I_0 is the mass per unit area of the plates, $I_0=b\int_{-h/2}^{h/2}\rho\left(z\right)\mathrm{d}z$. For convenience, we introduce the dimensionless quantities $X=\frac{r}{R}$, $W=\frac{w}{R}$, $\alpha=\frac{M^TR}{B}$, $\beta=\frac{N^TR^2}{B}$, $I=\frac{I_0R^2}{B}$, and $\lambda=\frac{R}{h}$. Then, the Lagrange function can be written as

$$l=\frac{B}{2}\left[I\left(\frac{\partial W}{\partial t}\right)^2-\left(\frac{\partial^2W}{\partial X^2}+\frac{1}{X}\frac{\partial W}{\partial X}\right)^2+2\left(1-\nu\right)\frac{1}{X}\frac{\partial W}{\partial X}\frac{\partial^2W}{\partial X^2}\right.$$

$$\left.-\alpha\frac{\partial^2W}{\partial X^2}-\alpha\frac{1}{X}\frac{\partial W}{\partial X}+\beta\left(\frac{\partial W}{\partial X}\right)^2\right]. \tag{8}$$

The dimensionless boundary conditions are expressed as

$$W\big|_{X=1}=0\quad\left.\frac{\partial W}{\partial X}\right|_{X=1}=0 \tag{9}$$

To introduce the problem into the Hamilton system, the differential expressions are defined as $\frac{\partial W}{\partial t}=\dot{W}$ and $\frac{\partial W}{\partial X}=W'$.

The relevant dual variable is $P=\frac{\delta l}{\delta\dot{W}}=I\dot{W}$. Inserting these expressions into Eq. (8), the Hamiltonian is written as

$$H\left(W,P\right)=P\dot{W}-l=\left(1-\frac{B}{2}\right)\frac{P^2}{I}+\frac{B}{2}\left[\left(\frac{\partial^2W}{\partial X^2}+\frac{1}{X}\frac{\partial W}{\partial X}\right)^2\right.$$

$$-2(1-\nu)\frac{1}{X}\frac{\partial W}{\partial X}\frac{\partial^2 W}{\partial X^2}+\alpha\frac{\partial^2 W}{\partial X^2}+\alpha\frac{1}{X}\frac{\partial W}{\partial X}-\beta\left(\frac{\partial W}{\partial X}\right)^2\Bigg].$$

According to the Hamilton principle, the canonical equations in the Hamilton system can be obtained by a variational process. In order to solve the canonical equations accurately and analytically, the variable $M=-B\left(\frac{\partial^2 W}{\partial X^2}+\frac{1}{X}\frac{\partial W}{\partial X}\right)$ was introduced. Then, the dual canonical equations in the Hamilton system was deduced in the form

$$\dot{\boldsymbol{\Psi}}=\begin{bmatrix}\dfrac{\delta H}{\delta M}\\ -\dfrac{\delta H}{\delta W}\end{bmatrix}\{\boldsymbol{\Psi}\}=\mathbf{H}\boldsymbol{\Psi}\,, \tag{10}$$

where $\boldsymbol{\Psi}$ and $\mathbf{H}$ are the state vector and the Hamilton operator respectively, which are defined as

$$\boldsymbol{\Psi}=\begin{Bmatrix}W\\ M\end{Bmatrix},\quad \mathbf{H}=\begin{bmatrix}\dfrac{1}{R^2}\dfrac{\partial}{\partial X}\left(X\dfrac{\partial}{\partial X}\right) & \dfrac{X}{B}\\ \beta\dfrac{\partial}{\partial X}\left(X\dfrac{\partial}{\partial X}\right) & -\dfrac{\partial}{\partial X}\left(X\dfrac{\partial}{\partial X}\right)\end{bmatrix}. \tag{11}$$

In Eq. (11), $\beta=\dfrac{N^T R^2}{B}$, and thus the thermal membrane forces N^T, which depend on temperature fields, are also considered. Therefore, solutions for the temperature fields have to be obtained before solving the canonical equations. According to the Fourier heat conduction theory, the heat conduction equation is written as

$$C(z)\rho(z)\frac{\partial T}{\partial t}=\frac{\partial}{\partial z}\left[K(z)\frac{\partial T}{\partial z}\right],\quad \left(t>0,-\frac{h}{2}<z<\frac{h}{2}\right). \tag{12}$$

The initial and boundary conditions are

$$T(z,0)=0\,,\quad T\left(-\frac{h}{2},t\right)=\Delta T\cdot f(t),\quad -K(z)\frac{\partial T}{\partial z}\bigg|_{z=h/2}=h_r T\left(\frac{h}{2},t\right), \tag{13}$$

where h_r is the heat exchange coefficient between the upper surfaces of the plates and the surrounding environment. Equations (12) and (13) were solved analytically using the Laplace transformation technique in combination with the power series method, which gave the transient temperature fields in the FGM circular plates under dynamic thermal loads. The solution process is the same as in [1], where the transient temperature fields of FGM cylindrical shells were determined.

3. Solutions of Canonical Equations

The analytical solution of Eqs. (10) and (12)is

$$\boldsymbol{\Psi}=C_1\begin{bmatrix}1\\ 0\end{bmatrix}+C_2\begin{bmatrix}\mathbf{J}_0(\sqrt{\beta}X)\\ \beta\mathbf{J}_0(\sqrt{\beta}X)\end{bmatrix}, \tag{14}$$

TABLE 1. Material Properties of Constituents

Material	k, W/(m·K)	ρ, kg/m^3	E, GPa	α, 1/K	C, J/(kg·K)
SiC	65.0	3100	427	$4.3\cdot10^{-6}$	670
Ni	90.5	8890	206	$13.3\cdot10^{-6}$	439.5

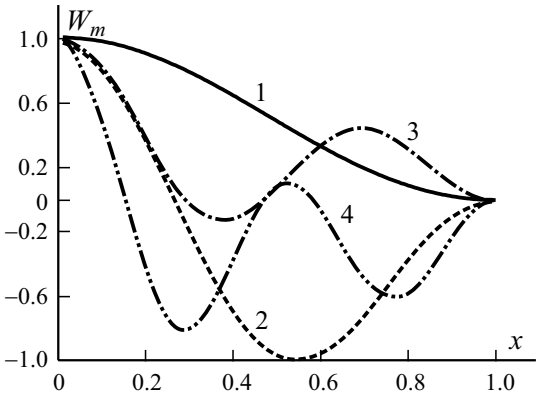

Fig.1. The first- (1), second- (2), third- (3), and fourth-order (4) buckling modes.

where $\mathrm{J}_0(\sqrt{\beta}X)$ is the primal Bessel function; C_1 and C_2 are coefficients. Inserting W into boundary conditions (9) gives

$$\begin{bmatrix} 1 & \mathrm{J}_0(\sqrt{\beta}) \\ 0 & -\sqrt{\beta}\mathrm{J}_1(\sqrt{\beta}) \end{bmatrix} \begin{Bmatrix} C_1 \\ C_2 \end{Bmatrix} = 0 \tag{15}$$

The solution of Eq. (15) has to be nonzero at the dynamic buckling of plates. Therefore, the determinant of the coefficient matrix of Eq. (15) has to be equal to zero, namely,

$$\begin{vmatrix} 1 & \mathrm{J}_0(\sqrt{\beta}) \\ 0 & -\sqrt{\beta}\mathrm{J}_1(\sqrt{\beta}) \end{vmatrix} = 0\,. \tag{16}$$

Expanding Eq. (16), the bifurcation condition is obtain as

$$\mathrm{J}_1(\sqrt{\beta}) = 0\,. \tag{17}$$

In combination with $\beta = \dfrac{N^T R^2}{B}$, the thermal membrane buckling forces are calculated by solving Eq. (17). Based on the expression $N^T = \dfrac{1}{1-\nu}\int_{-h/2}^{h/2} E(z)\alpha(z)T(z,t)\mathrm{d}z$, the relevant buckling temperature increments ΔT_m are obtained.

In order to determine buckling modes, we assume that $C_2 = C_m$. In addition, solving Eq. (15), it is found that $C_1 = -C_m \mathrm{J}_0\left(\sqrt{\beta}\right)$. Inserting C_1 and C_2 into Eq. (14), the buckling modal equation of the FGM circular plates is obtained in the form

$$W_m = C_m\left[-\mathrm{J}_0\left(\sqrt{\beta_m}\right) + \mathrm{J}_0\left(\sqrt{\beta_m}X\right)\right]. \tag{18}$$

TABLE 2. Comparison of Critical Buckling Temperature Increments ΔT_{cr}

Source	SiC	k						Ni
		0.5	1	2	5	10	100	
[23]	548.11	337.95	289.28	258.23	235.19	219.52	188.38	183.48
Present	555.34	349.91	305.54	275.28	246.12	225.81	190.95	185.92
Difference, %	1.30	3.42	5.32	6.19	4.44	2.79	1.35	1.31

TABLE 3. Buckling Temperature Increments ΔT_m of Plates under Exponential Thermal Loads

Material	Buckling mode		
	1	2	3
	$\beta_m = 14.59$	$\beta_m = 49.28$	$\beta_m = 103.43$
SiC	246.82	833.67	1749.73
$k = 0.5$	155.52	525.28	1102.47
$k = 1$	135.79	458.67	962.66
$k = 2$	122.34	413.24	867.32
$k = 5$	109.39	369.47	775.45
$k = 10$	100.36	338.97	711.45
$k = 100$	84.87	286.65	601.62
Ni	82.63	279.10	585.77

4. Numerical Results and Discussions

4.1. Buckling modes

In this Section, a numerical analysis and calculations are presented for FGM circular plates made of SiC and Ni. Table 1 lists the material properties of SiC and Ni. If not stated otherwise, the geometric dimensions of the plate are h = 1 cm, R = 30 cm, and $\lambda = \frac{R}{h} = 30$. Two kinds of thermal loads were considered separately in the calculation: an exponentially increasing thermal load and a one-step constant thermal load, i.e., $f(t) = 1 - e^{-at}$ and $f(t) = 1$. If not specified otherwise, Δt =5 s, $a = 10$, and $h_r = 50$.

Bifurcation conditions Eq. (17) were solved by the Newton–Raphson method. The following dimensionless eigenvalues were obtained:

$$\beta_1 = 14.59,\ \beta_2 = 49.28,\ \beta_3 = 103.43,\ \beta_4 = 177.42,\ \beta_5 = 271.26,\ \beta_6 = 384.94, \cdots.$$

Inserting β_m into Eq. (18), the buckling modes were found. The first- to fourth-order axisymmetric buckling modes of the plates are plotted in Fig. 1. As is seen, different eigenvalues correspond to different buckling modes. The order of buckling mode increased with growing dimensionless eigenvalues. At the same time, the shapes of buckling modes did not depend on material properties.

TABLE 4. Critical Temperature Increments ΔT_{cr} of Plates with Different λ

λ	20	25	30	35	40
SiC	555.34	355.42	246.82	181.34	138.84
$k = 0.5$	349.91	223.94	155.52	114.26	87.48
$k = 1$	305.54	195.54	135.79	99.77	76.38
$k = 2$	275.28	176.18	122.34	89.89	68.82
$k = 5$	246.12	157.52	109.39	80.37	61.53
$k = 10$	225.81	144.52	100.36	73.73	56.45
$k = 100$	190.95	122.21	84.87	62.35	47.74
Ni	185.92	118.99	82.63	60.71	46.48

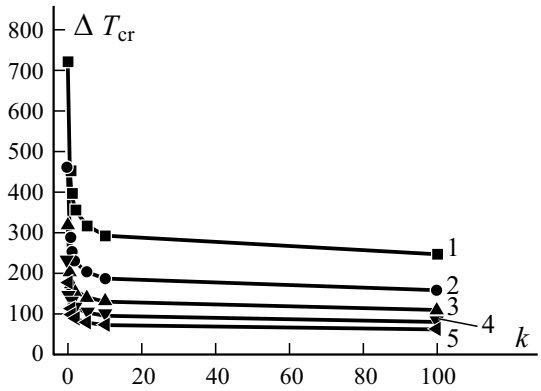

Fig.2. Critical temperature increments ΔT_{cr} of plates under a one-step thermal load versus k at λ = 20 (1), 25 (2), 30 (3), 35 (4), and 40 (5).

4.2. Increments of dynamic buckling temperature

In this Section, the dynamic buckling temperature increments are calculated and discussed, and the influence of material gradient, parameters of structural geometry and thermal loading on the critical buckling temperatures are studied. First, the effectiveness and accuracy of dynamic buckling analysis by the symplectic method are verified using linear perturbation method. A comparisons of the critical buckling temperature ΔT_{cr} for the plates under exponential thermal loadings with the corresponding results obtain in [23] are shown in Table 2, where the parameters $h = 1$ cm and $R = 20$ cm are the same as the relevant ones indicated in the literature. As is seen, the critical buckling temperature increments obtained by the symplectic method are very close to those found by the classical elasticity method.

Table 3 lists the first- to third-order buckling temperature increments ΔT_m for the plates subjected to the load of exponential type with different power-law indices k. It is seen that the buckling temperature increments differ greatly for the different orders of buckling modes, namely, the greater the buckling wave number, the higher the buckling thermal load is required. The critical buckling temperature increments, i.e., the minimum increments of buckling temperature are the eigenvalues corresponding to first-order buckling mode: $m = 1$. The instability of the FGM circular plates is axisymmetric, because the plates are subjected to uniformly distributed dynamic thermal loads.

TABLE 5. Critical Temperature Increments ΔT_{cr} for Some Specific Values of h_r

h_r	10	30	50	70
SiC	246.34	246.58	246.82	247.06
$k = 0.5$	155.18	155.35	155.52	155.68
$k = 1$	135.52	135.66	135.79	135.93
$k = 2$	122.12	122.23	122.34	122.46
$k = 5$	109.20	109.29	109.39	109.48
$k = 10$	100.19	100.27	100.36	100.44
$k = 100$	84.72	84.79	84.87	84.94
Ni	82.49	82.56	82.63	82.70

TABLE 6. Critical Buckling Temperature Increments ΔT_{cr} of Plates for Different Δt

Δt, c	1	2	5	10	∞
SiC	407.06	297.78	246.82	242.43	242.33
$k = 0.5$	303.63	210.12	155.52	146.38	145.72
$k = 1$	270.32	186.24	135.79	126.79	126.01
$k = 2$	243.18	167.64	122.34	114.20	113.53
$k = 5$	213.11	147.80	109.39	101.76	102.39
$k = 10$	191.45	133.69	100.36	95.03	94.68
$k = 100$	156.82	111.01	84.87	80.95	80.72
Ni	152.72	108.09	82.63	78.82	78.60

The effect of the power-law index k and the ratio of radius to thickness $\lambda = R/h$ on the critical buckling temperature increments of the plates under two kinds of dynamic thermal loads is shown in Table 4 and Fig. 2. Figure 2 illustrates relationships between the critical buckling temperature increments and k at different values of λ. As follows from Table 4 and Fig.2, the buckling temperature decreases if the power law index k increases. This means that, with increasing k, the ability of the plates to withstand dynamic thermal actions decrease. At $k < 2$, the decrease in buckling temperature increments is greater. However, the curves are leveling off when $k > 2$. This is because the FGM plates become homogeneous ceramic at $k = 0$ and metallic at $k \to \infty$. The concentration of ceramic drops when k increases, and Young's modulus and the bending stiffness decrease. In addition, the bending stiffness of the plates decreases when λ increases. Thus, the critical buckling temperature increments decreases significantly when λ increases.

The critical buckling temperature increments of the plates subjected to the exponential thermal loads, for some specific values of h_r, are listed in Table 5. As is seen, the critical buckling temperature increments do not depend on h_r. This means that the heat transfer coefficients have a small effect on the dynamic thermal buckling of FGM circular plates.

The critical buckling temperature increments at different loading times Δt are shown in Table 6 and Fig. 3. As is seen, the critical buckling temperature increments decrease with growing loading time. At $\Delta t < 5$ s, the critical temperature

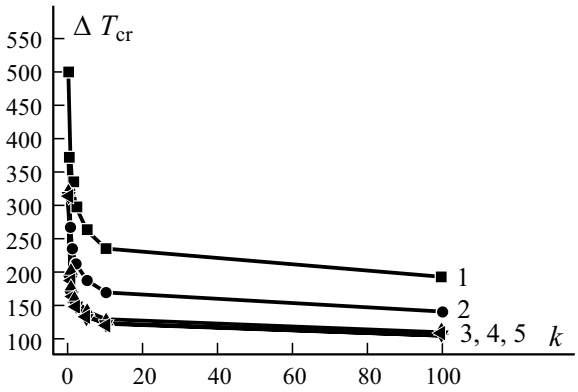

Fig. 3. Critical temperature increments ΔT_{cr} versus k for Δt = 1 (1), 2 (2), 5 (3), 10 (4), and 10,000 (5).

increments decreases drastically as the loading time is lengthened. But it hardly varies and tends to a constant with growing loading time if when $\Delta t > 5$ s. This is because the longer the process, the more uniform are temperature distributions inside the plates, and the influence of the buckling critical temperature gradually disappears as the loading time is lengthened.

5. Conclusions

The dynamic thermal buckling of the FGM circular plates was studied using the symplectic method in the Hamilton system. Canonical equations were established and solved analytically in the symplectic space, and then the complete buckling modes in terms of Bessel functions were obtained. Relationships between the critical loads and buckling modes on the one hand and the symplectic eigenvalues and eigensolutions on the other hand are revealed. The study performed shows the symplectic method can efficiently be used to investigate the dynamic thermal buckling problem of FGM structures. The gradient properties of functionally graded materials have great effects on the critical buckling temperatures. The critical buckling temperature increments decrease with increasing gradient parameter and can be changed by adjusting the volume fractions of constituent materials. The ratio of plate radius to thickness and the time of the dynamic loading greatly affect the critical temperatures, but the effect of heat transfer coefficient is small.

Acknowledgements. This work was supported by the National Natural Science Foundation of China [grants Nos.11662008 and 11862012] and the abroad exchange funding for young backbone teachers of Lanzhou University of Technology.

REFERENCES

1. J. H. Zhang, G. Z. Li, S. R. Li, and Y. B. Ma, "DQM-based thermal stresses analysis of a functionally graded cylindrical shell under thermal shock," J. Thermal Stresses, **38**, No. 9, 959-982 (2015).
2. B. Diveyev, I. Butyter, and Y. Pelekh, "Dynamic properties of symmetric and asymmetric Beams made of Functionally Graded materials in bending," Mech. Compos. Mater, **54**, No. 1, 111-118 (2018).
3. J. H. Zhang, S. C. Pan, and L. K. Chen, "Dynamic thermal buckling and postbuckling of clamped–clamped imperfect functionally graded annular plates," Nonlinear Dyn., **95**, 565-577 (2019).
4. S. R. Li, J. H. Zhang, and Y. G. Zhao, "Thermal post-buckling of functionally graded material Timoshenko beams," Appl. Math. Mech., **27**, No. 6, 803-811 (2006).
5. S. R. Li, J. H. Zhang, and Y.G. Zhao, "Nonlinear thermo-mechanical post-buckling of circular FGM plate with geometric imperfection," Thin-Wall. Struct., **45**, No.5, 528-536 (2007).
6. K. S. Anandrao, R. K. Gupta, P. Ramchandran, and G.V. Rao, "Thermal post-buckling analysis of uniform slender functionally graded material beams", Struct. Eng. and Mech., **36**, No. 5, 545-560 (2010).
7. G. L. She, F. G. Yuan, and Y. R. Ren, "Nonlinear analysis of bending, thermal buckling and post-buckling for functionally graded tubes by using a refined beam theory," Compos. Struct., **165**, 74-82 (2017).
8. G. L. She, F. G. Yuan, and Y.R. Ren, "Thermal buckling and post-buckling analysis of functionally graded beams based on a general higher-order shear deformation theory," Appl. Math. Model., **47**, 340-357 (2017).
9. L. S. Ma and T. J. Wang, "Nonlinear bending and post-buckling of a functionally graded circular plate under mechanical and thermal loadings," Int. J. Solids. Struct., **40**, No. 13-14, 3311-3330 (2003).
10. L. S. Ma and T. J. Wang, "Relationships between the solutions of axisymmetric bending and buckling of functionally graded circular plates based on the third-order plate theory and the classical solutions for isotropic circular plates," Int. J. Solids. Struct., **41**, No. 1, 85-101 (2004).
11. X. L. Jia, L. L. Ke, X. L. Zhong, Y. Sun, J. Yang, and S. Kitipornchai, "Thermal-mechanical-electrical buckling behavior of functionally graded micro-beams based on modified couple stress theory," Compos. Struct., **202**, 625-634 (2018)
12. J. Sun, X. Xu, and C.W. Lim, "Buckling of functionally graded cylindrical shells under combined thermal and compressive loads," J. Thermal Stresses, **37**, No. 3, 340-362 (2014).
13. J. Sun, X. Xu, and C. W. Lim, "Torsional buckling of functionally graded cylindrical shells with temperature-dependent properties," Int. J. Struct. Stab. Dy., **14**, No.1, 1350 048 (2014).
14. B. Mirzavand, M. R. Eslami, and M. Shakeri, "Dynamic thermal postbuckling analysis of piezoelectric functionally graded cylindrical shells," J. Thermal Stresses, **33**, No. 7, 646-660 (2010).
15. B. Mirzavand, M. R. Eslami, and J. N. Reddy, "Dynamic thermal postbuckling analysis of shear-deformable piezoelectric FGM cylindrical shells," J. Thermal Stresses, **36**, No. 3, 189-206 (2013).
16. M. Shariyat, "Dynamic thermal buckling of suddenly heated temperature-dependent FGM cylindrical shells under combined axial compression and external pressure," Int. J. Solids. Struct., **45**, No. 9, 2598-2612 (2008).
17. M. Shariyat, "Vibration and dynamic buckling control of imperfect hybrid FGM plates with temperature-dependent material properties subjected to thermo-electro-mechanical loading conditions," Compos. Struct., **88**, No. 2, 240-252 (2009).
18. D. H. Bich, D. Van Dung, V. H. Nam, and N.T. Phuong, "Nonlinear static and dynamic buckling analysis of imperfect eccentrically stiffened functionally graded circular cylindrical thin shells under axial compression," Int. J. Mech. Sci., **74**, 190-200 (2013).
19. K. Gao, W. Gao, D. Wu, and C. Song, "Nonlinear dynamic buckling of the imperfect orthotropic E-FGM circular cylindrical shells subjected to the longitudinal constant velocity," Int. J. Mech. Sci., **138**, 199-209 (2018).
20. C. W. Lim and X. S. Xu, "Symplectic elasticity: theory and applications," Appl. Mech. Rev., **63**, No. 5, 1-10 (2010).

21. X. Xu, H. Chu, and C.W. Lim, “A symplectic Hamiltonian approach for thermal buckling of cylindrical shells,” Int. J. Struct. Stab. Dy., **10**, No. 2, 273-286 (2010).
22. J. H. Zhang and S. R. Li, “Dynamic buckling of FGM truncated conical shells subjected to non-uniform normal impact load,” Compos. Struct., **92**, No. 12, 2979-2983 (2010).
23. J. H. Zhang, S. C. Pan, and S. R. Li, “Dynamic buckling of functionally graded circular plate under thermal shock,” Chinese J. of Applied Mechanics [in Chinese], **32**, No. 6, 901-907 (2015).